Dynamic mechanical analysis test for evaluating loose sands on a wide strain range application to the insight mission on mars

Lopez, María Juliana Chaparro; Castillo-Betancourt, Juan Pablo; Cabrera, Miguel; Caicedo, Bernardo; Delage, Pierre; Lognonné, Philippe; Banerdt, Bruce

DOI
10.1520/GTJ20230381

Publication date
2023

Document Version
Final published version

Published in
Geotechnical Testing Journal

ASTM INTERNATIONAL

Geotechnical Testing Journal

María Juliana Chaparro López,[1] Juan-Pablo Castillo-Betancourt,[2] Miguel Cabrera,[3] Bernardo Caicedo,[2] Pierre Delage,[4] Philippe Lognonné,[5] and Bruce Banerdt[6]

DOI: 10.1520/GTJ20230381

Dynamic Mechanical Analysis Test for Evaluating Loose Sands on a Wide Strain Range—Application to the InSight Mission on Mars

Geotechnical Testing Journal

doi:10.1520/GTJ20230381 available online at www.astm.org

María Juliana Chaparro López,[1] Juan-Pablo Castillo-Betancourt,[2] Miguel Cabrera,[3] Bernardo Caicedo,[2] Pierre Delage,[4] Philippe Lognonné,[5] and Bruce Banerdt[6]

Dynamic Mechanical Analysis Test for Evaluating Loose Sands on a Wide Strain Range—Application to the InSight Mission on Mars

Reference

M. J. Chaparro López, J.-P. Castillo-Betancourt, M. Cabrera, B. Caicedo, P. Delage, P. Lognonné, and B. Banerdt, "Dynamic Mechanical Analysis Test for Evaluating Loose Sands on a Wide Strain Range—Application to the InSight Mission on Mars," *Geotechnical Testing Journal* https://doi.org/10.1520/GTJ20230381

Manuscript received April 24, 2023; accepted for publication July 24, 2023; published online September 20, 2023.

[1] Department of Civil Environmental Engineering- Universidad de Los Andes, Carrera 1 No. 18A-12, Bogotá 111711, Colombia (Corresponding author), e-mail: mj.chaparro@uniandes.edu.co, https://orcid.org/0009-0004-7086-6026

[2] Department of Civil Environmental Engineering- Universidad de Los Andes, Carrera 1 No. 18A-12, Bogotá 111711, Colombia, https://orcid.org/0000-0003-3123-4654 (J.-P.C.-B.), https://orcid.org/0000-0003-4344-0914 (B.C.)

[3] Faculty of Civil Engineering and Geosciences- Delft University of Technology, Mekelweg 5, Delft 2628, the Netherlands, https://orcid.org/0000-0002-9236-8130

ABSTRACT

The dynamic properties of loose sands under low stresses are an unexplored topic in soil dynamics because these soil conditions are uncommon in most geotechnical structures on Earth. However, low densities and low-stress conditions prevail on other planets, like, for instance, the surface of Mars, for which particular attention is presently given through the InSight NASA mission. This work presents a new procedure for measuring the dynamic properties of loose sand under low stress by using the dynamical mechanical analysis (DMA) tester, a technique commonly used in asphalt engineering but not in geotechnical engineering. Compared to traditional geotechnical methods (resonant column and cyclic triaxial tests), DMA investigates a broader range of strains using a single apparatus. In this work, we assess the dynamical properties of loose fine sand $D_r \approx 0.2$, considered a possible Mars regolith analog, by varying the input strain from $\gamma = 10^{-6}$ to $\gamma = 10^{-2}$ while applying confining pressures from $\sigma_3 = 3$ kPa to $\sigma_3 = 30$ kPa. The results validate the proposed procedure, showing an increment of the shear modulus as the confining pressure increases. Furthermore, they highlight DMA's advantages for studying the dynamic properties of granular soils under low stress and strain.

Keywords

dynamic properties, dynamical mechanical analysis, rheometer, loose sand, Martian simulant, low confining pressure

[4] Laboratoire Navier–Centre d'Enseignement et de Recherche en Mécanique des Sols (CERMES) - École des Ponts ParisTech, 6-8 Avenue Blaise-Pascal, Marne-la-Vallée 77420, France, https://orcid.org/0000-0002-2101-5522

[5] Université Paris-Cité, Institut de Physique du Globe de Paris, Rue Jussieu, Paris, Paris 75006, France, https://orcid.org/0000-0002-1014-920X

[6] Jet Propulsion Laboratory, NASA–CalTech, 4800 Oak Grove Dr., Pasadena, CA 91125, USA, https://orcid.org/0000-0003-3125-1542

Nomenclature

C_u = uniformity coefficient
D_{50} = median particle size
D_r = relative density
e = void ratio
G = dynamic shear modulus
G_{max} = maximum dynamic shear modulus
T = torque
σ = standard deviation
σ_3 = confining pressures
σ_v = basal suction
ξ = damping ratio
ρ = grain density
θ = rotation reported by the rheometer
τ = shear stress
γ = shear strain
γ_e = shear strain in the elastic threshold
γ_r = reference shear strain
ψ = suction

Introduction

The study of the dynamic properties of Martian regolith gained interest because of NASA's InSight mission on Mars (Interior Exploration using Seismic Investigations, Geodesy, and Heat Transport). InSight is a geophysical mission that successfully installed for the first time on the surface of Mars, in an area called Elysium Planitia, a high-sensitivity, very large band seismometer called SEIS (Seismic Experiment for Interior Structure), together with a self-driving thermal probe called HP3 (Heat Flow and Physical Properties Package). Both instruments provided detailed geophysical and mechanical data of the near-surface terrain. **Figure 1** presents a photo taken at the beginning of the mission by the instrument context camera of the InSight lander, showing that the landing site, called Homestead Hollow, is flat and characterized by a sandy deposit with little rock abundance as planned from orbiter data during the landing site selection (Golombek et al. 2020). **Figure 1** also shows, in the center, the semispherical white wind and thermal shield covering the SEIS seismometer to protect it from Martian winds (under an average atmospheric pressure of 600 Pa) and temperature changes (between −20°C and −80°C). The selection of the Martian regolith simulants was based on orbital thermal inertia measurements, geological considerations, and some observations from former rover missions (Golombek et al. 2008), suggesting that the Mars surface in Elysium Planitia is made up of loose subrounded to rounded sand with an average diameter of around $D_{50} = 175$ μm.

The physical properties of the surface regolith were further characterized by local thermal measurements conducted with the HP3 probe, which indicated a low thermal conductivity for the upper 3–37 cm of the soil (0.039 ± 0.002 W m^{-1} K^{-1}) from which quite a low density was derived, around 1.2 Mg/m^3 (Spohn et al. 2018). The very low-stress profile along the first 10 cm is related to the low gravity on Mars (3.73 m/s^2).

On Mars, regolith grains are rounded because of long-term saltation by Martian winds, as directly observed by Goetz et al. (2010) through optical microscope observations

FIG. 1 Instrument context camera view of the wind and thermal shield (WTS) covering the SEIS seismometer in the center and the HP3 device on the left-hand side. The foot consists of a disc with 60-mm diameter and a 20-mm-long conic spike (10-mm diameter at its base) in its center (Image Credit: NASA/JPL-Caltech: _mars.nasa.gov_insight-raw-images_surface_sol_1436_icc_C000M1436_724026383EDR_F0000_0200M_).

onboard the Phoenix spacecraft. Previous studies showed that the NE34 Fontainebleau sand could be a proper Martian regolith simulant (Delage et al., forthcoming). Fontainebleau sand is a well-sorted silica sand (grain density $\rho_s = 2.651$ Mg/m^3) from the Paris Basin with a D_{50} of 220 μm, compared with the $D_{50} = 175$ μm diameter derived from thermal inertia measurements.

Previous investigations on Martial regolith allowed providing some first estimates of the compression and shear velocities of Mars's surface (Delage et al. 2017), together with other physical properties (Spohn et al. 2018), the interaction between the SEIS foot and the Martian regolith (Delage et al., forthcoming) and the study of the shear and compressive wave's velocity and Poisson ratio, among others.

Given that little information is available about the shear modulus degradation curve in sands below $\sigma_3 =$ 30 kPa, a new specific device, using a DMA rheometer, was used to investigate very low stresses. This article describes this new system and the tests carried out to investigate the degradation curve of the shear modulus at very low stresses and from low to large shear strains.

Background

Cyclic loading is a load repeatedly applied with a specific frequency (Ishihara 1996). Cyclic loading is of practical relevance for many problems in geotechnical engineering on Earth and other planets (e.g., Mars). It may be caused by human activities, like traffic, or natural sources, like seismic loads leading to the propagation of shear waves in the soil and inducing cyclic shearing (Wichtmann 2016). The dynamic shear modulus G and the damping ratio ξ characterized the soil response to cyclic and dynamic loadings. The soil response depends on the soil characteristics (e.g., relative density, grain size distribution), and conditions (e.g., confining pressure and strain level) (Kramer 1996).

Ishibashi and Zhang (1993) analyzed the dynamic properties of G and ξ of available soil set experimental data, including nonplastic sands to highly plastic clays, evaluating the effects of plasticity and confining pressure σ_3. The research concludes that the plastic index (PI) is the main factor controlling stiffness for plastic soils. In contrast, for cohesionless soils, like sands, the confining pressures significantly affect the soil stiffness (Molina-Gómez et al. 2020).

In terms of confining pressure, it influences the mechanical behavior of soil. The maximum shear modulus G_{max} for granular materials strongly depends on the confining pressure σ_3. This dependency is usually analyzed through the general form of equation (1) (Molina-Gómez et al. 2020):

$$G_{max} = C\left(\frac{\sigma_3}{P_a}\right)^n f(e) \tag{1}$$

where C is a material coefficient that captures the influence of the particle shape and bonding or cementation of the particles, P_a is the atmospheric pressure, and n is a power exponent that reflects the sensitivity of the stiffness modulus to the confining pressure, and $f(e)$ is a void ratio function (Molina-Gómez et al. 2020).

The dependency between the maximum shear modulus and confining pressure σ_3 determines that the level of soil resistance decreases when the confining pressure is low. In consequence, the understanding of soil behavior at low stress is essential to geotechnical engineering problems related to shallow foundations, slope stability with a risk of surface failure, tunnels with shallow overburdens, geotechnical structures subjected to static or cyclic loading under low confining stress (Huang et al. 2015), or the effect of seismic wave register by the SEIS (Delage et al., forthcoming).

Researchers have developed several laboratory and field tests throughout history to assess how confining pressure σ_3 and strain levels γ affect a soil's mechanical properties G and ξ, evaluating different strain ranges and minimum confining pressures.

Regarding the confining pressure effect on soil properties, test procedures have been developed to evaluate the effect of low confining pressures; however, the dynamic properties (G, ξ) have been measured at a minimum confining pressure of $\sigma_3 = 20$ kPa. Delfosse-Ribay et al. (2004) evaluated both G and ξ in a resonant column (RC) test on a natural Fontainebleau sand ($D_{50} = 220$ μm) and mixtures with various grouting materials (Delfosse-Ribay et al. 2004). They showed that, for all materials, the confining pressure improves the shear modulus, with, however, a negligible effect on the damping ratio. More recently, Kumar, Krishna, and Dey (n.d.) investigated the dynamic properties (G, ξ) of sand and sandy soil with fines in a confining pressure range $\sigma_3 = [20:300]$ kPa. They point out that both G and ξ are significantly affected by the confining pressure, showing that an increase in the confining pressure increases G and decreases ξ, with a significant increase in cyclic strength under higher confining pressures (Kumar, Krishna, and Dey n.d.). Delage et al. (2017, forthcoming) investigated dry sand's dynamic properties (G, ξ) at confining pressures $\sigma_3 \geq 20$ kPa and relative densities $D_r \geq 0.3$. In this research, RC and triaxial tests were used to explore the influence of previbration cycles at two relative densities ($D_r = [0.3,0.6]$) and two confining pressures ($\sigma_3 = [100, 300]$ kPa). The results showed a slight decrease in shear modulus with increased loading cycles, with a significant drop in damping ratio. In addition, increased confining pressure decreases the sand's damping ratio and reduces the effect of the number of previbration cycles. More recently, Molina-Gómez et al. (2020) presented a detailed characterization of two historically liquefiable sands from the greater Lisbon area using bender elements and RCs evaluating a confining pressure range of $\sigma_3 = [30–200]$ kPa. The results showed that the damping ratio increases with strain level in the range $\gamma > 10^{-5}$ in both sands. Furthermore, results showed that ξ decreases as σ_3 increases. Despite the existing research, few of them explore the very low-stress range $\sigma_3 \leq 30$ kPa.

Alternatively, the loading frequency repetition and the strain level significantly impact the soil's response to dynamic loads. The strain magnitude determines the soil phenomena and the mechanical characteristics (Ishihara 1996). Generally, soil deformations in a range of $\gamma < 10^{-5}$ are elastic and recoverable; the associated phenomenon could be the vibration and wave propagation through the soil layer. In contrast, in a range of $\gamma = [10^{-4}–10^{-2}]$, the soil behavior is elasto-plastic, producing irrecoverable deformation. In this condition, the development of cracks or differential settlements appears. Also, for strains $\gamma > 10^{-2}$, the soil could suffer slides, compaction, or liquefaction at higher strain levels (Ishihara 1996).

The strain level effect is evaluated in different ranges depending on the device and test characteristics (see **Table 1**). Generally, in-situ measurements include vibration tests evaluating strain ranges of $\gamma = [10^{-5}–10^{-3}]$ and seismic wave method evaluating ranges of $\gamma = [10^{-6}–10^{-5}]$ (Ishihara 1996). Laboratory tests have a wide range of

TABLE 1
Shear strain ranges for soil dynamics tests measuring the shear modulus degradation

Test Method	Strain Level
Rheometer	10^{-6}:10^{-2}
Bender elements	10^{-6}:10^{-5}
Resonant column	2×10^{-6}:6×10^{-3}
Repeated loading test (e.g., cyclic triaxial test)	10^{-4}:10^{-2}
Combined methods: Torsional shear + electromagnetic	10^{-6}:10^{-2}

strain levels. The bender elements measure the elastic material zone. These tests could measure the strain range of $\gamma = [10^{-6}–10^{-5}]$ (Ishihara 1996; Rio 2006; Irfan et al. 2020). The elastic zone and part of the elasto-plastic zone of the shear modulus degradation curve could be measured by the RC, which provides information in the strain range of $\gamma = [2{\times}10^{-6}{:}6{\times}10^{-3}]$ (Ishihara 1996; Molina-Gómez et al. 2020). The elasto-plastic zone properties could be measured by repeated loading tests, like the dynamic triaxial test, which measures higher strain levels ($\gamma \geq 10^{-4}$) evaluating the shear dynamic modulus G degradation. Also, devices like the cyclic direct simple test, provide strain data between the RC and the triaxial test $\gamma = [10^{-4}{:}10^{-3}]$, measuring the maximum dynamic shear modulus G_{max} at the limit of the elastic range.

In order to measure the entire elastic and elastoplastic strain range, combined methods have been developed. For example, The University of Texas at Austin developed the fixed free RC/torsional shear (RCTS) studying the behavior of geomaterials at shear strain ranging from $\gamma = [10^{-5}{:}10^{-3}]$ (d'Onofrio, Silvestri, and Vinale 1999). Based on the design criteria of the RCTS, d'Onofrio, Silvestri, and Vinale (1999) developed a resonant column/torsional shear device (THOR), a new torsional shear apparatus composed of a torsional cyclic shear device incorporating an electromagnetic loading system with a high-resolution measurement system allowing better precision measurements at strain levels below $\gamma < 10^{-5}$ (d'Onofrio, Silvestri, and Vinale 1999). However, finding a single instrument suitable for measuring strains within the entire allowable range $\gamma = [10^{-6}{:}10^{-2}]$ was not possible. Consequently, two different transducers had to be used. Hence, rotations were monitored by a pair of microproximity and approximators (d'Onofrio, Silvestri, and Vinale 1999).

The combination of the existing devices allows the evaluation of soil's elastic and elasto-plastic behavior in a strain range of $\gamma = [10^{-6}{:}10^{-2}]$. However, a single curve could not be guaranteed in all cases because of differences in the loading setups, the sample preparation, and the deformation measurements (Villacreses et al. 2020). Therefore, using one single device over a wide strain range $\gamma = [10^{-6}{:}10^{-2}]$ appears useful and can be achieved with an oscillating rheometer, often used in other engineering fields (asphalt engineering or food processing).

The dynamical mechanical analysis (DMA) dynamic shear rheometer measures a shear strain range of $\gamma = [10^{-6}{:}10^{-2}]$. It applies a harmonic oscillatory stress or strain signal with a controlled frequency and strain amplitude, measuring the material dynamic properties G and ξ (Villacreses et al. 2020). **Table 1** shows a summary of the strain level ranges that some devices could measure based on the references analyzed (Ishihara 1996; d'Onofrio, Silvestri, and Vinale 1999; Rio 2006; Irfan et al. 2020; Molina-Gómez et al. 2020; Villacreses et al. 2020). The rheometer test used in this research is a single device (not a combined method) that can measure a whole strain range from 10^{-6} to 10^{-2}.

Villacreses et al. (2020) tested kaolin samples in the DMA and subjected the samples to different suction conditions $\psi = [0.35–98.5]$ MPa measuring a shear strain range of $\gamma = [6{\times}10^{-6}{:}1{\times}10^{-3}]$. The authors compared G and ξ with results obtained with the resonant-column apparatus, proving that the proposed method (DMA) could measure the soil behavior in a wider strain range and identify a G_{max} close to the value reported by the RC.

The results obtained by Villacreses et al. (2020) suggest that DMA had better precision than available tests for fine-grained soils. However, evaluating the dynamic soil properties of granular soils using DMA is challenging as dry granular soils require a confining pressure for holding the sample. Therefore, a careful preparation method is needed to ensure a uniform relative density across the sample.

The existing tests methods evaluate different strain ranges and confining pressures. However, a single device to evaluate the soil mechanical properties (G and ξ) for loose sands in a strain range of $\gamma = [10^{-6}–10^{-2}]$ and under low confinement pressures ($\sigma_3 < 10$ kPa) is currently missing. Also, the soil behavior under dynamic loads at low confining pressures requires further investigation. Therefore, this study introduces a novel procedure using the DMA for loose dry sand, enabling the determination of dynamic parameters (G and ξ) across a wide strain range of $\gamma = [10^{-6}{:}10^{-2}]$ varying confining pressures $\sigma_3 = [3–30]$ kPa.

Experimental Observations on Cyclic Degradation

To the author's knowledge, the first study points to soil modulus degradation measurements dating back to the mid-1930s with the RC works of Ishimoto (Ishimoto and Iida 1936). However, the first documented observations relating shear strain with the shear modulus degradation in soils date back to the decade of the 1960s. In this decade, the dynamic characteristics were measured using standard devices, like the cyclic triaxial or the RC. First, the triaxial test measured the hysteresis loop of several coarse-grained soils (Weissman and Hart 1962). Next, the effect of variables such as the void ratio and the degradation of the wave velocity was evaluated using the RC on sands (Hardin and Richart 1963). Then, the observations of shear modulus degradation sparked the attention of the geotechnical community between 1966 and 1972, when the first degradation curves for the G moduli, on both sands and clays, were presented (Drnevich, Hall, and Richart 1966; Silver and Seed 1969; Seed 1970; Hardin and Drnevich 1972). Numerous works followed these early steps, relating the cyclic degradation in clays with the plasticity index. Similarly, for materials such as Toyoura sand, the presentation of the cyclic degradation in terms of normalized moduli G/G_{max} allowed a simpler comparison (Kokusho 1980; Vucetic and Dobry 1991).

The sample confining stress affects the degradation curves, showing a significant variation under slight variations in confinement. At stresses below $\sigma_3 = 100$ kPa, curves for different tests may be mixed, highlighting the relevance of test repeatability concerning the values' variability (Darendeli 2001).

Another key question lies in the interpretation of the degradation curve curvature. Semi-empirical fitting models that recreate the moduli degradation phenomena have addressed this question. These models are generally formulated regarding the normalized modulus as a function of the shear strain imposed upon the soil (Hardin and Drnevich 1972; Darendeli 2001).

Ishibashi and Zhang (1993) collected available data on dynamic shear moduli of various nonplastic sands and compared the data with a general equation for sandy soil relating the shear modulus with the confining pressure, expressed as equation (2).

$$\begin{aligned} \frac{G}{G_{\max}} &= K(\gamma)\sigma_3^{-m(\gamma)-m_0} \\ K(\gamma) &= 0.5\left[1+\tanh\left\{\ln\left(\frac{0.000102}{\gamma}\right)^{0.492}\right\}\right] \\ m(\gamma)-m_0 &= 0.272\left[1-\tanh\left\{\ln\left(\frac{0.000556}{\gamma}\right)^{0.4}\right\}\right] \end{aligned} \tag{2}$$

Ishibashi and Zhang (1993) also established an equation for the damping ratio related to G/G_{max}. However, the author mentioned that because measurements of damping ratio are more sensitive and challenging than the shear modulus measurements G and large damping ratios ξ would not be attained until the final stages of dynamic computations, the scatter of the data points was considered small, and it was fitted by equation (3) (Ishibashi and Zhang 1993).

$$\xi = 0.333\left\{0.586\left(\frac{G}{G_{\max}}\right)^2 - 1.547\left(\frac{G}{G_{\max}}\right) + 1\right\} \tag{3}$$

Besides the relation between the G_{max} and the confining pressure σ_3, the modified hyperbolic model is a general model that describes the shear modulus reduction of fine and granular soils. Santos and Gomes Correia (2001) investigate the shear modulus degradation of soil with strain. The study was based on a key parameter

defined previously by the authors and called reference threshold shear strain $\gamma_{0.7}$. This parameter was defined as the shear strain for a normalized soil stiffness degradation factor of $G/G_{max} = 0.7$, in which G_{max} is the initial shear modulus for a very small strain ($\gamma = 10^{-6}$), and G is the secant modulus of soil. The authors proposed a hyperbolic function used to fit test results. Simple regression analysis shows that the previous boundary curves can be fitted by a mean curve defined by the following relationship shown in equation (4). The best fitting was obtained with $a = 0.385$ based on the least squares method.

$$\frac{G}{G_{\max}} = \frac{1}{1 + a\left(\frac{\gamma}{\gamma_{0.7}}\right)} \tag{4}$$

More recently, Oztroprak and Bolton (2013) calibrated the model's parameter to fit the results of 454 literature tests on granular soils. In addition, the model parameters were found based on a detailed review of an extensive experimental data collection for sands with various grain size distributions (Oztroprak and Bolton 2013). Based on these calibrations, the model yields a relatively simple equation (5).

$$\frac{G}{G_{\max}} = \frac{1}{\left[1 + \left(\frac{\gamma - \gamma_e}{\gamma_r}\right)^a\right]} \tag{5}$$

where the normalized soil stiffness G/G_{max} can be estimated as a function of the shear strain γ, a reference shear strain γ_r an elastic threshold strain γ_e, and a curvature coefficient α, varying between 0.75 to 1.0 (Oztroprak and Bolton 2013).

According to the authors, the model may be used with G_{max} values directly measured from one of the experimental tests. Another option is to use it with the usual power models to predict the initial modulus value. The authors report that this model yields better predictions for higher strain values, and as is often the case, it has a significant uncertainty for low strains and stress values.

Materials and Methods

The DMA test is commonly used for determining the viscoelastic material properties of asphalt mixtures, like dynamic shear modulus and phase angle at different temperatures (Caro, Sánchez, and Caicedo 2015). The technique is also recommended for evaluating the deterioration of asphalt materials and their performance with temperature control (Caro, Sánchez, and Caicedo 2015). The test involves applying a harmonic oscillatory angular strain with frequency and amplitude control while measuring the necessary stress for maintaining the harmonic motion and the sample rotation with a precision of 10^{-9} N.m and 40 nrad, respectively (TA Instruments 2006). The measuring principle of the DMA is like the cyclic torsional test currently used to characterize cyclic soil behavior.

The DMA test directly and precisely measures the dynamic shear modulus G and damping ratio ξ. In this work, we adapt the DMA test by allowing basal suction σ_v and, hence, applying a confining pressure σ_3 to a dry sand sample (see **fig. 2**). In consequence, this procedure extends the experimental capabilities of the DMA to coarse-grained materials, allowing the study of the dynamic properties in a wider range of deformations and all in a single test.

This method's advantage is its ability to evaluate the dynamic soil response under a strain range $\gamma = [10^{-6}–10^{-2}]$ using a single device. Additionally, the rheometer provides precise values for each strain level with high accuracy. However, this procedure is specifically designed for dry sands with low confining pressures. To use this method on saturated sands, a system that blocks water from the vacuum system is required.

FIG. 2 Schematic of the DMA for dry sands. (*A*) Experimental setup: photograph of the DMA tester with a zoom of the sample; (*B*) sample dimensions, coupling system, and basal confinement.

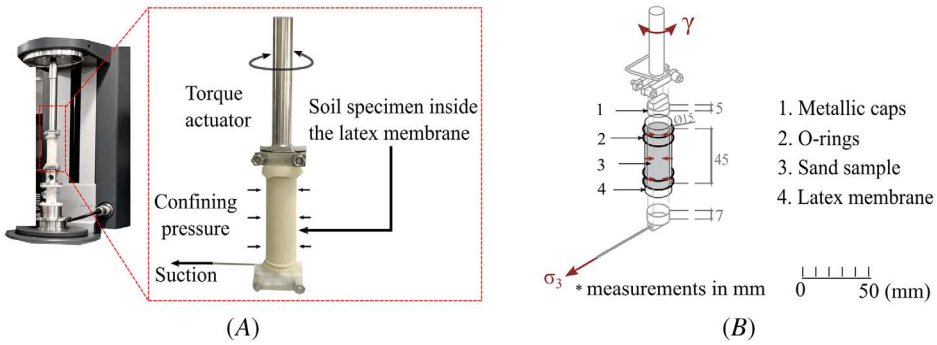

SYSTEM DEVICE

Rheometers that apply cyclic signals of strains are known as DMA testers (Villacreses et al. 2020). The shear rheometer employed in this work has a minimum torque oscillation of 3×10^{-8} N.m and a minimum torque steady of 5×10^{-8} N.m. It could apply a minimum torque of 0.2 N.m, with a resolution of 1×10^{-9} N. Also, the motor has an inertia of 15 μ N.m.s and can apply an angular velocity in a range of 1×10^{-8} rad/s to 3×10^{-2} rad/s, with a displacement resolution of 4×10^{-5} rad (TA Instruments 2006; Villacreses et al. 2020).

In the shear rheometer, the sample is held on two metallic caps, tightened by two O-rings, and enclosed by a hand-made latex membrane. Initially, the piston directly contacts the sample, and the membrane is fitted onto the cap. Although the membrane may introduce additional confining stress, this effect can be disregarded when the vacuum is applied, as the membrane becomes stress-free. However, in larger deformations where the specimen is fully degraded, the membrane remains embedded in the cap, resulting in recorded shear corresponding to the membrane. The confining pressure system is activated through a miniature hole on the bottom cap (see fig. 2). The DMA has a series of automated testing modes, among which the sweep shear strain is selected in this work.

The system device components have been designed especially for this test. First, the hand-made latex membrane is made using a rigorous proceeding with a smooth wood mold and submerged in liquid latex. The bottom and top caps are made of aluminum, matching the rheometer pedestal diameter. A rigid slice pipe of polyvinyl chloride supports the latex membrane while the sand sample is prepared. Table 2 shows the dimensions of the shear rheometer components.

TABLE 2
System device components dimensions and materials

Components	Dimensions	Material
Bottom and top cap	Diameter: 15 mm	Aluminum
Membrane	Diameter: 15 mm	Latex
	Height: 60 mm	
	Thickness: 2 mm	
Rigid slice pipe	Diameter: 15 mm	Polyvinyl chloride
	Height: 45 mm	
	Thickness: 3 mm	
O-rings	Diameter: 15 mm	Rubber
	Thickness: 1 mm	

MATERIAL

Selecting a relevant Martian regolith simulant is challenging (Seiferlin et al. 2008). However, based on the measurements of the microscopic images of the Mars exploration rovers and Mars science laboratory, based on Phoenix missions, and by thermal inertia measurement, the Insight mission team has decided on Fontainebleau sand (NE34), a well-sorted rounded sand with an average grain diameter of $D_{50} = 220$ μm (close to 170 μm, which is the estimated value at the InSight site) (Delage et al., forthcoming). Golombek et al. (2020) presented a geological description of the so-called 'homestead hollow' where the lander is located. Based on it, the Insight research team estimated the cross-section of the landing site with a layer around 3 m thick of relatively fine-grained impact-generated regolith that is likely to grade with depth into coarse, blocky ejecta, which overlies fractured basalt flows, with an estimated 10-m-thick layer of blocky ejecta (Golombek et al. 2020; Delage et al., forthcoming).

Because one of the objectives in this research is evaluating the applicability of the DMA method on the Martian simulant regolith, experiments are performed on Fontainebleau sand, with a nearly monodisperse grain size distribution, mean grain diameter of $D_{50} = 220$ μm, uniformity coefficient $C_u = 1.52$, void ratio range of $[e_{min}: e_{max}] = [0.54: 0.84]$, and grain density of $\rho_s = 2.65$ g/cm^3 (Delage et al., forthcoming). **Figure 3** shows the grain size distribution obtained following the procedure of ASTM D6913, *Standard Test Methods for Particle-Size Distribution (Gradation) of Soils Using Sieve Analysis*.

SAMPLE PREPARATION

The sample preparation is the most critical and challenging step because of the sample's small dimensions and low density. The preparation process is carefully controlled, so replicability for all samples is guaranteed.

The DMA samples are prepared within a latex membrane and encapsulated within a rigid sliced pipe (see **fig. 4A**). The sliced pipe controls the sample dimensions, resulting in a sample of 15 mm in diameter. The space between the rheometer pedestal and the piston restricts the sample height to 45 mm (see **Table 2**). The membrane is external to the system comprising the sample and the metallic caps. That is why when the rheometer piston goes down, it touches the sample directly.

Regarding the sample size, the proposed method applies only to fine sands. In fact, as noted in Gourves and Mezghani (1988), Gourves (1993), and Caicedo (2018), a relationship between the diameter of the sample and the maximum particle size sample $d_{sample}/D_{max} > 10$ is required to reach a coefficient lower than 10 % in contact forces between particles. In this research, such a relationship is 375, ensuring that the sample behaves as a continuum.

The preparation procedure is as follows. First, the latex membrane is embedded in the bottom cap using two O-rings. Then, the rigid pipe covers the latex membrane giving support while the sample is prepared. Next, the sand is pluviated into the membrane using a funnel with a diameter of 5 mm. The funnel goes down until the bottom cap and the sand is deposited into the funnel. Then the funnel is raised, ensuring a release height close to zero. This process is essential in maintaining minimal external vibrations on the sample and avoiding possible densification. For control purposes, sample density is measured after the test, weighing the sand within the latex membrane, and obtaining variations of density of up to +/− 0.05 g/cm^3. Once the sample reaches the required

FIG. 3

Grain distribution obtained of Fontainebleau Sand. Inset: Photograph of the sand sample.

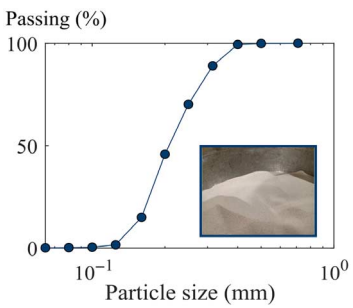

FIG. 4 Schematics of the (*A*) sample preparation and (*B*) water column method for a better precision measuring the confining pressure. 1. Sample in the rheometer's pedestal; 2. suction through the cap hole; 3. water column–ruler; 4. water-sand trap, 5. pressure gauge; and 6. building's vacuum system.

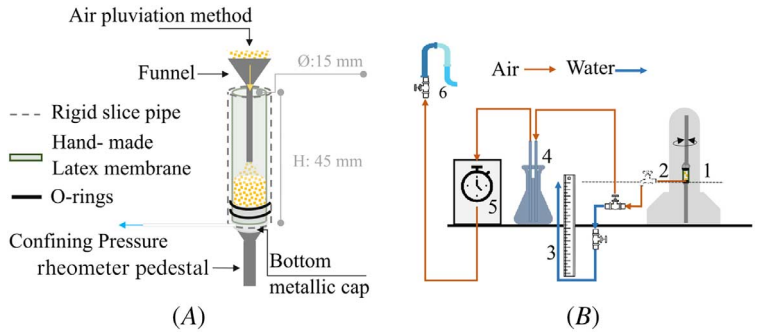

density, the top rheometer motor is downed close to the sample. It is essential that the motor does not touch the sample and densifies it. Next, the latex membrane is tightened to the top and bottom DMA caps by two O-rings, ensuring a joined motion during the test (see fig. 4*B*). Once the sample height is reached and both caps are tight, air suction is applied through the bottom cap, inducing a confining pressure σ_3 on the sample. Special care is devoted to inspecting for air leakages on the membrane fixtures or the membrane.

Low-confining pressures are controlled with a 100-mbar suction pump (reference: AGA VALVULA-EVAC 1000). For pressures below $\sigma_3 = 10$ kPa, we employed a water column method, guaranteeing a better precision measurement (see fig. 4*B*). In this process, the suction pump applies the confining pressure required through an air pipe joined to the bottom cap, but as the pressure is low, an additional method is necessary to regulate the measurement. First, the air pipe is bound to a water pipe using a water trap. Then, the water pipe allows the measurement of the water level, corresponding to the confining pressure applied. For pressures higher than $\sigma_3 = 10$ kPa, the suction can be applied directly by the suction pump, obtaining better precision values with a precision of +/− 0.01 kPa.

EXPERIMENTAL CAMPAIGN

The DMA tests are conducted on a Fontainebleau sand with a relative density of $D_r = 0.2$ +/− 0.05, subjected to a strain range of $\gamma = [10^{-6}{:}10^{-2}]$ and maintain a constant shear strain rate frequency of $f = 1$ Hz over 10 harmonic signals. The frequency value was determined using a sweep frequency test to evaluate the frequency effect. Figure 5 shows the results of a frequency sweep test in a range of $f = [0.01–8]$ Hz at a confining pressure of $\sigma_3 = 5$ kPa and a constant strain level of $\gamma = 0.0004$. This confining pressure was selected because it allows the evaluation of the effects of the frequency effects at very low confining pressure. Figure 5 shows that the frequency differs, showing a frequency effect. Because of this research following a shear strain sweep test, a constant frequency of $f = 1$ Hz was selected as the constant value.

FIG. 5

Frequency sweep test for a confining pressure of $\sigma_3 = 5$ kPa at a constant strain level of $\gamma = 0.0004$.

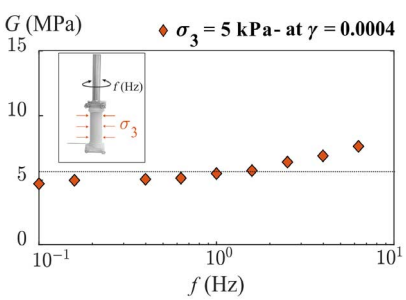

The DMA test using the rheometer is carried out using a strain sweep methodology that applies a sinusoidal torsional strain signal with a period of 1 min while the oscillation stress is recorded. This research tests the sand samples with a strain/displacement control. Each sweep strain test consists of 13 strain levels in the range values of $\gamma = [10^{-6}{:}10^{-2}]$, applying 10 harmonic sinusoidal signals with a period of 1 min (see fig. 6). This procedure is adapted from the DMA test on kaolin samples by Villacreses et al. (2020).

The strain values increase during the test proportionally with piston rotation θ. Then, this rotation is converted into strain values according to the sample diameter and height. Besides the rotation, the DMA rheometer reports the values of the torque (T) applied to the sample in values of micro-Newton meters; these values are the basis of the shear stress calculation τ. Finally, the experimental variable is the confining pressure, whereas the strain range, density, and dimensions remain constant.

The adapted DMA allows testing the sand sample to very low confining pressures, like $\sigma_3 = 3$ kPa, until raising it to $\sigma_3 = 30$ kPa. For each confining pressure level, a total sweep shear strain is performed. Each confining pressure has three repetitions, confirming the test repeatability for DMA test. A sample is prepared for each confining pressure and test repeatability; once the swipe strain test ends, the system device is disassembled, cleaned, and assembled for the new test. Table 3 summarizes the experimental campaign. The harmonic signal is recorded for each strain level step. This is the base of the hysteretic loop, which is the basis for determining the

FIG. 6 Scheme of the test campaign.

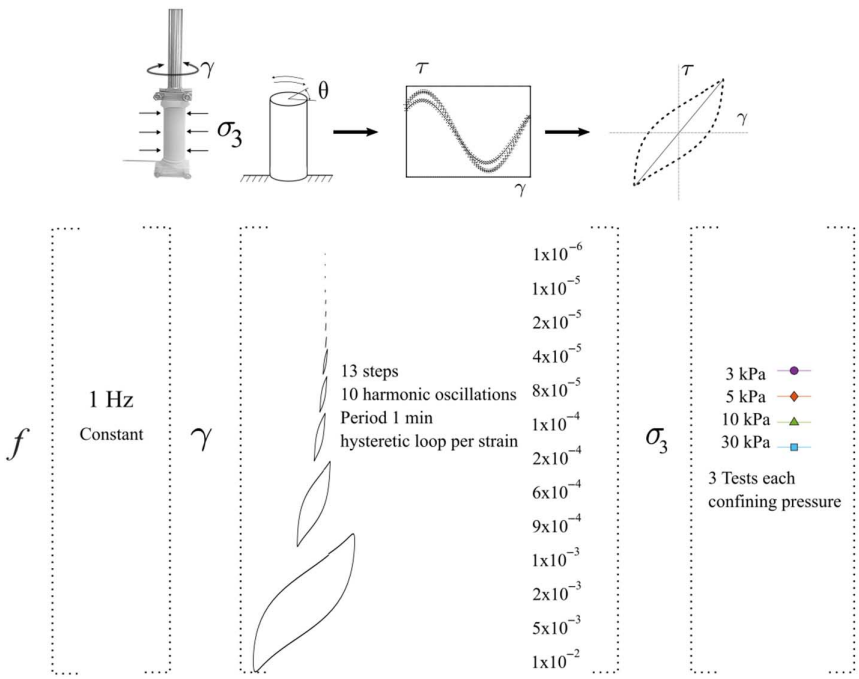

TABLE 3
Experimental campaign

Parameter	Dimensions	Material	Condition
Sample condition	Diameter: 15 mm Height: 45 mm	Fontainebleau sand	Dry relative density: ≈ 0.2
	Swipe strain range	Frequency	Confining pressure
Test condition	$[10^{-6}{:}10^{-2}]$ Constant	1 Hz Constant	$\sigma_3 = [3, 5, 10, 30]$ kPa

dynamic properties G and ξ. **Figure 6** shows how the hysteretic loop area increases as the strain level increases and how the hysteretic loop slope decreases.

Results and Discussion

The sand's dynamic mechanical properties, G and ξ, can be evaluated using the harmonic signals recorded by the DMA rheometer. The recorded signals show a clean harmonic motion in time and allow the reconstruction of the hysteretic loop for each confining pressure (see **fig. 7**).

The hysteretic loops are recorded for each strain level, starting with the first strain level reported on the sample until the last strain level. **Figure 8*A*** shows the variation of the hysteretic loops for a confining pressure of $\sigma_3 =$ 30 kPa. The hysteretic loops size increase as the strain level increases. In contrast, the hysteresis loop slope decreases along the swipe strain test. **Figure 8*B*** shows the hysteretic loop for the first strain level recorded ($\gamma = 5.2\times10^{-7}$). Comparing the first hysteretic loop with the lasted hysteretic loops ($\gamma \geq 1\times10^{-3}$), the loop area is significantly higher for the last loop, showing a material energy dissipation during the test. The DMA test measured the properties of the first hysteretic loop, indicating that it can measure the sample's elastic range at the initial strain levels.

DYNAMIC SHEAR MODULUS

The hysteretic loop is the base of the dynamic measurements. Its slope depends on the soil stiffness G (see inset **fig. 9*A***), which can be described by equation (6).

FIG. 7 Example of a single oscillation recorded in the DMA test. (*A*) Shear stress and strain harmonic and (*B*) hysteretic loop for strain levels of $\gamma = 0.003$ and $\gamma = 0.001$ when the sample is subjected at $\sigma_3 = 30$ kPa.

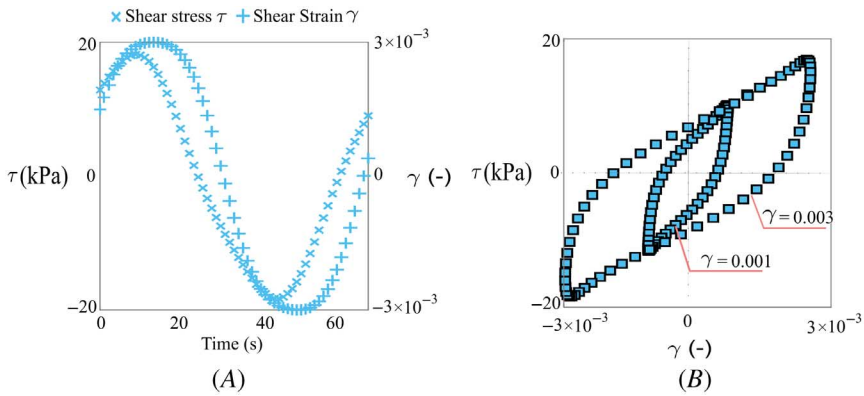

FIG. 8

(*A*) Variation of the hysteretic loops for a confining pressure of $\sigma_3 = 30$ kPa. (*B*) Zoom in the first strain level.

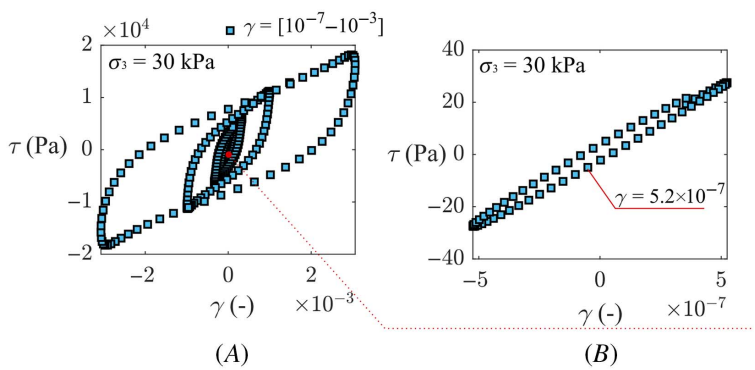

FIG. 9

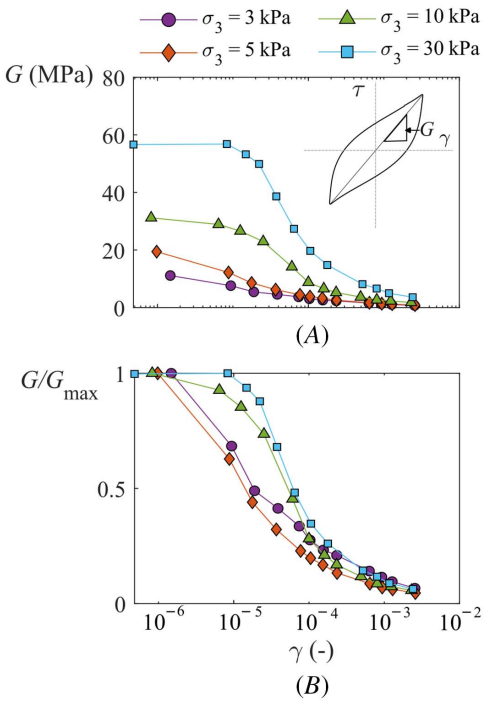

Shear modulus G degradation curve. (*A*) Evolution of G as a function of γ for confining pressures of $\sigma_3 = [3, 5, 10, 30]$ kPa at $f = 1$ Hz. Inset: Hysteretic loops for the same confining pressures at a shear strain level of $\gamma = 0.0010$. (*B*) Normalized shear modulus G/G_{max} as a function of γ.

$$G = \frac{\tau}{\gamma} \tag{6}$$

where τ is the shear stress related to the torque applied on the sample, and γ is the shear strain amplitude observed as the sample rotates (Kramer 1996).

The sweep strain test $\gamma = [10^{-6}–10^{-2}]$ is carried out for confining pressure $\sigma_3 = [3, 5, 10, 30]$ kPa with the three repetitions per confining pressure value. **Figure 9** shows the mean value of the shear modulus obtained in each strain step and each confining pressure. **Figure 9*A*** shows the shear modulus evolution as the confining pressure increase, and **figure 9*B*** shows the shear modulus degradation for each confining pressure. As shown in **figure 9*A***, the maximum shear modulus increase as the confining pressure increases. This stiffness increase is attributable to the increment in the hysteretic loop slope (see **fig. 9*A*** inset). For example, for $\sigma_3 = 3$ kPa, the hysteresis loop has a slope close to zero because the material is loose, and the confining pressure is low.

In contrast, for $\sigma_3 = 30$ kPa, the hysteresis loop inclination rises, pointing to a material stiffening and densification. The material is confined in this condition, and the elastic range extends to a strain level of $\gamma = 2\times10^{-5}$. The elastic range is evident for confining pressures of $\sigma_3 = 30$ kPa and $\sigma_3 = 10$ kPa; in these conditions, the material has more stiffness allowing a recoverable strain range. In contrast, as the confining pressures decrease, the material suffers a sudden degradation; hence, an elastic range is not evident for a confining pressure of $\sigma_3 = 3$ kPa, and the G curve is almost linear. In contrast, an evident effect of low confining pressures is a relatively lower dynamic shear modulus G and normalized modulus G/G_{max} (see **fig. 9*B***). However, the degradation rate increases as the confining pressure decreases, as $\sigma_3 = 30$ kPa has the highest slope, followed by $\sigma_3 = 10$ kPa and $\sigma_3 = 5$ kPa. The degraded curve for $\sigma_3 = 3$ kPa does not present an evident elastic range and is suddenly degraded.

In all cases, the relationship between G and G/G_{max} with γ shows degradation at moderately large strains. Interestingly, this degradation is observed on very low γ for low confining pressures $\sigma_3 = 3$ kPa, whereas it only initiates at $\gamma \geq 2\times10^{-5}$ for $\sigma_3 = 30$ kPa. Here, it is assumed that the sand stiffness is minimal under low

confinement, and the first oscillatory movement already degrades it. For this reason, the degradation curves for low confinement are linear, and an elastic range is not noticeable. Following the reasoning of an elasto-plastic material, the yield strain could set the transition between the elastic and the plastic ranges. This transition can be interpreted from the dynamic shear modulus degradation curve, and it can be argued that it depends on the confining pressure.

The results show that the degradation curve for 3 kPa points to a minimal elastic range from the test beginning and rapidly transitions to plastic behavior. On the other hand, the degradation curve of 30 kPa is more hyperbolic, or sigmoid, because of the transition from the elastic to the plastic range.

For a better precision degradation curve, it is helpful to compare the obtained results with the models proposed by Ishibashi and Zhang (1993) (equation (2)), Santos and Gomes Correia (2001) (equation (3)), and Oztoprak and Bolton (2013) (equation (4)). **Table 4** shows the nonlinear adjustment coefficient R^2. This coefficient of determination R^2 is a standard measure of goodness of fit for mathematical models fitted to empirical data using least squares regression (Kvålseth 1983). Kvålseth (1983) established that equation (7) is an appropriate measure of better precision for both linear and nonlinear models:

$$R^2 = 1 - \frac{\sum (G_{model} - \bar{G})^2}{\sum (G_{model} - G)^2} \tag{7}$$

where G_m are the fitted values obtained with the model, $\bar{G}$ is the mean value of the experimental results, and G is the experimental shear modulus obtained with the DMA test. Following this statement, a good fitting is determined by the closeness of R^2 to 1.

The results show that Oztoprak and Bolton's (2013) model fit well with confining pressures higher than 10 kPa. In contrast, for lower confining pressure, the fitting decreases. Hence, the Oztoprak and Bolton model works better when a yield strain is evident, creating the need in future works to adapt the model for describing those materials under low confinement and with a minimal elastic range. However, Ishibashi and Zhang (1993) and Santos and Gomes Correia (2001) still work for confining pressures $\sigma_3 \geq 5$ kPa, as the adjustment coefficients are close to $R^2 = 0.8$. **Figure 10** shows the degradation curves fitting with the theoretical models. The theoretical results validate the experimental results. For example, the Ishibashi and Zhang (1993) equation model directly relates the $G_{\max}$ with the confining pressure, and this model presents the best fitting. Hence, these results demonstrate the capability of the DMA test to measure the dynamic shear modulus at low confining pressures.

Besides the model agreement, the DMA methodology shows repeatability in the results. Each confining pressure was repeated three times. To evaluate the repeatability capability of the DMA, a correlation coefficient is calculated for each confining pressure. The correlation coefficient is a quantity that gives the quality of the least squares fitting to the original data. The correlation coefficient is used to determine the degree of association of variables. In multivariate experimentation (e.g., with three variables), it is often desirable to choose one's experiment. A convenient way of summarizing many correlation coefficients is to put them in a single table, called a correlation matrix. The correlation of any variable with itself is necessarily 1. Thus, the diagonals of the matrix are

TABLE 4

Coefficient of determination R^2 for the experimental degradation curves G/G_{max} at confining pressures $\sigma_3 = [3, 5, 10, 30]$ kPa fitting with theoretical models

	R^2		
σ_3 Confining Pressure Test, kPa	Fitting with Ishibashi and Zhang (1993)	Fitting with Santos and Gomes Correia (2001)	Fitting with Oztoprak and Bolton (2013)
3	0.6	0.7	0.6
5	0.8	0.8	0.6
10	0.8	0.9	0.9
30	0.9	0.9	0.8

FIG. 10

Degradation curves G/G_{max} at confining pressures $\sigma_3 = [3, 5, 10, 30]$ kPa fitting with theoretical models Ishibashi and Zhang (1993); Santos and Gomes Correia (2001); Oztoprak and Bolton (2013).

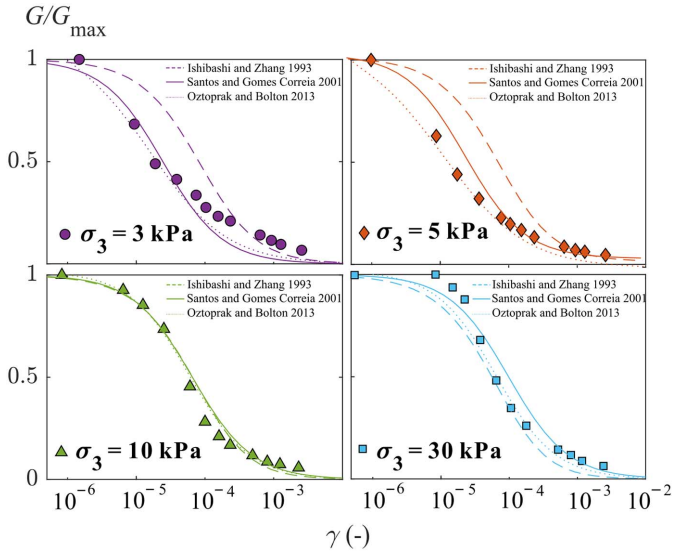

TABLE 5

The correlation coefficient for the three repetitions of the confining pressures $\sigma_3 = [3, 5, 10, 30]$ kPa

	3 kPa				5 kPa		
	Test 1	Test 2	Test 3		Test 1	Test 2	Test 3
Test 1	1.00			Test 1	1.00		
Test 2	0.97	1.00		Test 2	0.98	1.00	
Test 3	0.98	0.92	1.00	Test 3	1.00	0.99	1.00
	10 kPa				30 kPa		
	Test 1	Test 2	Test 3		Test 1	Test 2	Test 3
Test 1	1.00			Test 1	1.00		
Test 2	1.00	1.00		Test 2	0.99	1.00	
Test 3	0.98	0.99	1.00	Test 3	0.97	0.98	1.00

the unity, and as the correlation is close to 1, the data are similar, and the test device has high repeatability (Asuero, Sayago, and González 2006). The DMA results for each confining pressure present high correlation values (higher than 0.9), showing the DMA's repeatability capability. **Table 5** shows the correlation matrix for each test and confining pressure.

Additionally, test series under confining pressures of $\sigma_3 = [3, 5, 10, 30]$ kPa present a standard deviation (σ) lower than $\sigma = 0.17$ for the degradation curve. Also, the degradation shape is preserved, showing an elastic range at the beginning and a transition at $\gamma = 9\times10^{-5}$, then the dynamic shear modulus degrades (see **fig. 11**).

The reliability of the DMA results is measured with the reference results obtained by Molina-Gómez et al. (2020). In this research, a RC test was carried out on liquefied sand, on the TP-Lisboa sand with the same mean diameter as the Fontainebleau sand ($D_{50} = 0.22$ mm). The RC test was carried out in dry sand with a relative density of $D_r = 0.3$ for confining pressures in a range of $\sigma_3 = [30–200]$ kPa (Molina-Gómez et al. 2020). **Figure 12** shows the comparison between the DMA results and the RC results for a confining pressure of $\sigma_3 = 30$ kPa obtained by (Molina-Gómez et al. 2020). The Fontainebleau has a higher degradation rate as it has less density than the TP-Lisboa sand. However, the results present standard deviations σ between the shearing strain levels lower than $\sigma = 15$ MPa in the shear modulus curve.

FIG. 11

Test repetitions for shear modulus degradation curves for confining pressures of $\sigma_3 = [3, 5, 10, 30]$ kPa.

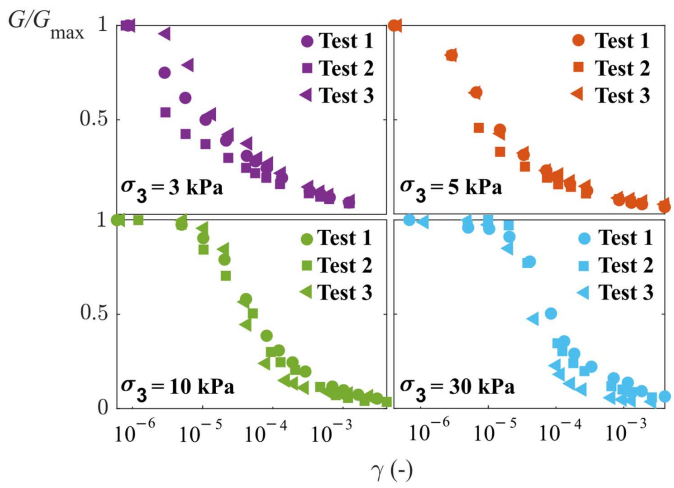

FIG. 12

Comparison between Fontainebleau sand tested in the DMA in dry condition with a relative density of D_r~0.2, and dry TP Lisboa Sand results using RC with a relative density of $D_r = 0.3$ +/−0.05.

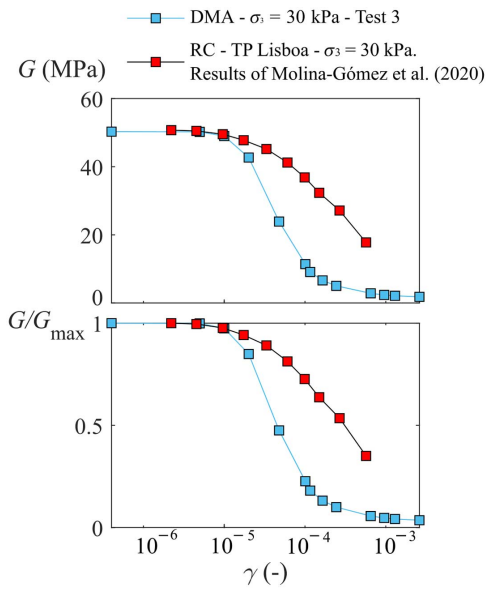

DAMPING RATIO

The repeated shearing on the sand sample produces an energy loss that is related to an accumulation of plastic strains (Kramer 1996). An alternative for accounting for this energy dissipation is the hysteretic loop area (see the shaded area in **fig. 13**). Both energy loss and dissipation are associated with the soil damping ratio ξ by the equation (8):

$$\xi = \frac{W_D}{4\pi W_s} = \frac{A_{loop}}{2\pi G\gamma^2} \tag{8}$$

where W_D is the dissipated energy, W_S is the maximum strain energy, and A_{loop} is the hysteretic loop area (Ishihara 1996 and Kramer 1996).

FIG. 13

Damping ratio ξ at confining pressures of $\sigma_3 = [3, 5, 10, 30]$ kPa at a cycle frequency of 1 Hz. Inset: Hysteretic loops showing definition of the elastic stored energy and dissipation energy.

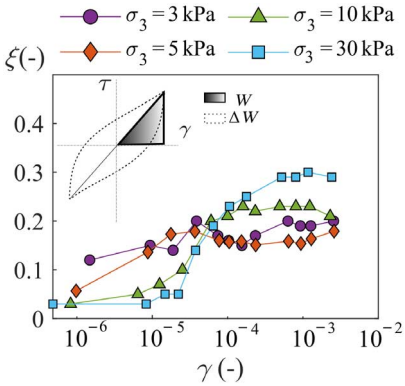

In a swipe strain test, at a constant confining pressure, the inner hysteretic loop area increases by increasing γ, representing a more significant energy dissipation as the sand is degraded (see **fig. 13**). As shown in **figure 13**, the material under low confining pressures ($\sigma_3 = 3$ kPa) has a lower degradation of ξ compared with higher confining pressures ($\sigma_3 = 30$ kPa). The curve for $\sigma_3 = 3$ kPa is less pronounced and falls between $\xi = 0.05$ and $\xi = 0.11$. However, the degradation is more significant for higher confining pressures ($\sigma_3 = 30$ kPa) and initiates for $\gamma > 10^{-5}$. As shown in **figure 13**, when the material is confined by $\sigma_3 = 30$ kPa, the damping ratio curve has an upward pick after a strain level of $\gamma = 10^{-4}$. This behavior relates to the dynamic shear modulus degradation described in **figure 9**. In contrast, for $\sigma_3 = 3$ kPa, the sand degradation can be assumed to occur under low-shear strains without showing a clear elastic range. Therefore, the damping ratio increment for $\sigma_3 = 3$ kPa is barely noticeable. However, the damping ratio for $\sigma_3 = 10$ kPa and $\sigma_3 = 30$ kPa increases as the sand is degraded (see **fig. 13**). For $\sigma_3 = 5$ kPa, the elastic range is seen slightly, but after a strain level of $\gamma = 10^{-5}$ behaves like $\sigma_3 = 3$ kPa.

According to the theory for soil damping ratio (Delage et al. 2017, forthcoming), the results for $\sigma_3 = 10$ kPa and $\sigma_3 = 30$ kPa show an expected behavior, with the stiffness increasing as the confining pressure increases and the damping ratio presenting a symmetrical behavior with the shear strain. However, for $\sigma_3 = 3$ kPa, results show that the damping ratio increases linearly with strains, and the damping ratio is around 6 % for low strains. This behavior constitutes a new finding of this study, which was observed thanks to the higher precision of the DMA under low confinements. The results show that using the DMA for sand allows the evaluation of the degradation curve in a wider strain range and the possibility to carry out tests at very low stress than the traditional methods.

FIG. 14

The damping ratio results $\sigma_3 = [3, 5, 10, 30]$ kPa compared with the theoretical model proposed by Ishibashi and Zhang (1993). Coefficient of determination $R^2 = [0.33, 0.35, 0.54, 0.85]$.

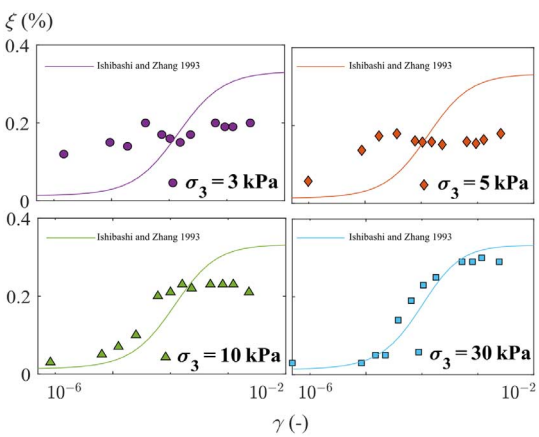

The damping ratio results are compared with the model proposed by Ishibashi and Zang (1993) (equation (2)). **Figure 14** shows the comparison between the theoretical model and the experimental results. For $\sigma_3 = [3, 5, 10, 30]$ kPa, the coefficient of determination R^2 obtained corresponds to $R^2 = [0.33, 0.35, 0.54, 0.85]$, proving that the theoretical model fit with the experimental damping ratio for confining pressures higher than $\sigma_3 \geq 30$ kPa, and highlight the limitations for a better precision fitting for lower confining pressures.

Conclusions

To better understand the dynamic parameters of the surface layer of regolith at the InSight landing site on Mars, an investigation of the dynamic properties of a regolith analog made up of subrounded loose Fontainebleau sand was carried out under stress and strain ranges significantly lower than in current practice in terrestrial soil mechanics. For his purpose, a DMA tester was used to evaluate the dynamic mechanical properties (shear dynamic modulus G and damping ratio ξ) of a sand loose sample ($D_r \approx 0.2$) submitted to confining pressures between $\sigma_3 =$ 3 kPa to $\sigma_3 = 30$ kPa at a frequency of $f = 1$ Hz. The experience shows that the DMA allows for high precision and good control of the shearing cycle. This characteristic allowed a better precision determination of the hysteretic loop. In addition, using the rheometer in the geotechnical field proved simple and better precision, allowing for evaluating the dynamic properties of a loose sand sample at very low confining pressures in a wider strain range compared to traditional methods and all within a single soil test.

The results validated the new procedure, highlighting its ease of preparation, high precision, and versatile control of both frequency and amplitude. In addition, it was observed that the confining pressure controlled the shear modulus degradation, evidencing an elastic zone for a confining pressure of $\sigma_3 = 30$ kPa and a total degradation at lower confining pressures, like $\sigma_3 = 3$ kPa. Each confining pressure was tested at least three times, with similar values of the maximum dynamic modulus for each test and similar curve shapes.

The yield strain (an essential parameter of the shear degradation), clearly observed under high confining pressure, disappeared under low confinement. Further work is necessary to explore its link with the confining pressure in more detail. Also, the degradation rate and maximum shear modulus are related to the confining pressure. The material stiffness influences the soil damping. The damping ratio ξ increment for $\sigma_3 = 3$ kPa and $\sigma_3 = 5$ kPa is barely noticeable. Conversely, the damping ratio for $\sigma_3 = 30$ kPa and $\sigma_3 = 10$ kPa increases as the sand is degraded.

The theoretical models can capture the modulus degradation curve when the material is confined at $\sigma_3 =$ 30 kPa, as a yield strain is evident. However, for a confinement pressure of $\sigma_3 = 3$ kPa and $\sigma_3 = 5$ kPa, the models do not slightly miss the range under low strains and do not have the best fitting. This shows the need for adapting the model to low confining pressures in further works. As a result, a comprehensive analytical framework could be elaborated for describing the degradation curves under a wider range of confinement pressures.

Finally, the new data obtained on the regolith analog now must be used in conjunction with the wave transfer at the surface of Mars to improve the analysis of the waves detected by the SEIS seismometer.

ACKNOWLEDGMENTS

The authors would like to thank Eng. Jose Naranjo from Universidad de Los Andes for his ideas and technical support in the design and elaboration of the experiment. Also, the authors are grateful for the financial support provided by Universidad de Los Andes, Colombia.

References

ASTM International. 2017. *Standard Test Methods for Particle-Size Distribution (Gradation) of Soils Using Sieve Analysis*. ASTM D6913(2017). West Conshohocken, PA: ASTM International, approved April 15, 2017. https://www.astm.org/d6913-04r09e01.html

Asuero, A. G., A. Sayago, and A. G. González. 2006. "The Correlation Coefficient: An Overview." *Critical Reviews in Analytical Chemistry* 36, no. 1 (January): 41–59. https://doi.org/10.1080/10408340500526766

Caicedo, B. 2018. *Geotechnics of Roads: Fundamentals*. Boca Raton, FL: CRC Press.
Caro, S., D. B. Sánchez, and B. Caicedo. 2015. "Methodology to Characterize Non-standard Asphalt Materials Using DMA Testing: Application to Natural Asphalt Mixtures." *International Journal of Pavement Engineering* 16, no. 1 (January): 1–10. https://doi.org/10.1080/10298436.2014.893328
Darendeli, M. B. "A New Family of Normalized Modulus Reduction and Material Damping Curves." PhD diss., The University of Texas at Austin, 2001.
Delage, P., J. P. C. Betancourt, B. Caicedo Hormaza, F. Karakostas, E. De Laure, P. Lognonné, D. Antonangeli, and B. Banerdt. Forthcoming. "The Interaction between the SEIS Seismometer of the InSight Martian Mission and a Regolith Simulant." *Géotechnique*. Published ahead of print, May 10, 2022. https://doi.org/10.1680/jgeot.21.00171
Delage, P., F. Karakostas, A. Dhemaied, M. Belmokhtar, P. Lognonné, M. Golombek, E. De Laure, et al. 2017. "An Investigation of the Mechanical Properties of Some Martian Regolith Simulants with Respect to the Surface Properties at the InSight Mission Landing Site." *Space Science Reviews* 211, no. 1 (February): 191–213. https://doi.org/10.1007/s11214-017-0339-7
Delfosse-Ribay, E., I. Djeran-Maigre, R. Cabrillac, and D. Gouvenot. 2004. "Shear Modulus and Damping Ratio of Grouted Sand." *Soil Dynamics and Earthquake Engineering* 24, no. 6 (August): 461–471. https://doi.org/10.1016/j.soildyn.2004.02.004
d'Onofrio, A., F. Silvestri, and F. Vinale. 1999. "A New Torsional Shear Device." *Geotechnical Testing Journal* 22, no. 2 (June): 107–117. https://doi.org/10.1520/GTJ11269J
Drnevich, V. P., J. R. Hall, and F. E. Richart. 1966. *Large Amplitude Vibration Effects on the Shear Modulus of Sand, Report No. 3-161*. Vicksburg, MS: US Army Waterways Experiment Station, Corps of Engineers.
Goetz, W., W. T. Pike, S. F. Hviid, M. B. Madsen, R. V. Morris, M. H. Hecht, U. Staufer, et al. 2010. "Microscopy Analysis of Soils at the Phoenix Landing Site, Mars: Classification of Soil Particles and Description of Their Optical and Magnetic Properties." *Journal of Geophysical Research: Planets* 115, no. E8 (August): E00E22. https://doi.org/10.1029/2009JE003437
Golombek, M. P., A. F. C. Haldemann, R. A. Simpson, R. L. Fergason, N. E. Putzig, R. E. Arvidson, J. F. Bell III, and M. T. Mellon. 2008. "Martian Surface Properties from Joint Analysis of Orbital, Earth-Based, and Surface Observations." In *The Martian Surface: Composition, Mineralogy, and Physical Properties*, edited by J. Bell, 468–498. Cambridge, UK: Cambridge University Press.
Golombek, M. P., N. H. Warner, J. A. Grant, E. Hauber, V. Ansan, C. M. Weitz, N. Williams, et al. 2020. "Geology of the InSight Landing Site on Mars." *Nature Communications* 11, no. 1 (February): 1014. https://doi.org/10.1038/s41467-020-14679-1
Gourves, R. 1993. "Application of the Schneebli Model in the Study of Micromechanics of Granular Media." *Mechanics of Materials* 16, nos. 1–2 (August): 125–131. https://doi.org/10.1016/0167-6636(93)90035-P
Gourves, R. and F. Mezghani. 1988. "Micromécanique des Milieux Granulaires, Approche Expérimentale Utilisant le Modèle de Schneebeli." *Revue Francaise de Geotechnique* 4 (October): 23–34. https://doi.org/10.1051/geotech/1988042023
Hardin, B. O. and V. P. Drnevich. 1972. "Shear Modulus and Damping in Soils: Design Equations and Curves." *Journal of the Soil Mechanics and Foundations Division* 98, no. 7 (July): 667–692. https://doi.org/10.1061/JSFEAQ.0001760
Hardin, B. O. and F. E. Richart Jr. 1963. "Elastic Wave Velocities in Granular Soils." *Journal of the Soil Mechanics and Foundations Division* 89, no. 1 (February): 33–65. https://doi.org/10.1061/JSFEAQ.0000493
Huang, Y., H. L. Cheng, T. Osada, A. Hosoya, and F. Zhang. 2015. "Mechanical Behavior of Clean Sand at Low Confining Pressure: Verification with Element and Model Tests." *Journal of Geotechnical and Geoenvironmental Engineering* 141, no. 8 (April): 06015005-1–06015005-6. https://doi.org/10.1061/(ASCE)GT.1943-5606.0001330
Irfan, M., G. Cascante, D. Basu, and Z. Khan. 2020. "Novel Evaluation of Bender Element Transmitter Response in Transparent Soil." *Geotechnique* 70, no. 3 (March): 187–198. https://doi.org/10.1680/jgeot.17.P.256
Ishibashi, I. and X. Zhang. 1993. "Unified Dynamic Shear Moduli and Damping Ratios of Sand and Clay." *Soils and Foundations* 33, no. 1 (March): 182–191. https://doi.org/10.3208/sandf1972.33.182
Ishihara, K. 1996. *Soil Behaviour in Earthquake Geotechnics*, 1st ed. Oxford, UK: Clarendon Press.
Ishimoto, M. and K. Iida. 1936. "Determination of Elastic Constants of Soils by Means of Vibration Methods: Part I. Young's Modulus." *Bulletin of Earthquake Research Institute* 14 (September): 632–656.
Kokusho, T. 1980. "Cyclic Triaxial Test of Dynamic Soil Properties for Wide Strain Range." *Soils and Foundations* 20, no. 2 (June): 45–60. https://doi.org/10.3208/sandf1972.20.2_45
Kramer, S. L. 1996. *Geotechnical Earthquake Engineering*. Uttar Pradesh, India: Pearson Education India.
Kumar, S. S., A. M. Krishna, and A. Dey. n.d. "Parameters Influencing Dynamic Soil Properties: A Review Treatise." Paper presented at the National Conference on Recent Advances in Civil Engineering, Nirjuli, India, January 2013.
Kvålseth, T. O. 1983. "Note on the R^2 Measure of Goodness of Fit for Nonlinear Models." *Bulletin of the Psychonomic Society* 21, no. 1 (January): 79–80.
Molina-Gómez, F., A. Viana da Fonseca, C. Ferreira, and J. Camacho-Tauta. 2020. "Dynamic Properties of Two Historically Liquefiable Sands in the Lisbon Area." *Soil Dynamics and Earthquake Engineering* 132 (May): 106101. https://doi.org/10.1016/j.soildyn.2020.106101
Oztoprak, S. and M. D. Bolton. 2013. "Stiffness of Sands through a Laboratory Test Database." *Géotechnique* 63, no. 1 (January): 54–70. https://doi.org/10.1680/geot.10.P.078
Rio, J. F. "Advances in Laboratory Geophysics Using Bender Elements." PhD diss., University College of London, 2006.
Santos, J. A. and A. Gomes Correia. 2001. "Reference Threshold Shear Strain of Soil. Its Application to Obtain an Unique Strain-Dependent Shear Modulus Curve for Soil." In *Proceedings of the 15th International Conference on Soil Mechanics and Geotechnical Engineering*, 267–270. London: International Society for Soil Mechanics and Geotechnical Engineering.

Seed, H. B. 1970. *Soil Moduli and Damping Factors for Dynamic Response Analyses, Report EERC-70*. Berkeley, CA: University of California, Berkeley.

Seiferlin, K., P. Ehrenfreund, J. Garry, K. Gunderson, E. Hütter, G. Kargl, A. Maturilli, and J. P. Merrison. 2008. "Simulating Martian Regolith in the Laboratory." *Planetary and Space Science* 56, no. 15 (December): 2009–2025. https://doi.org/10.1016/j.pss.2008.09.017

Silver, M. L. and H. B. Seed. "The Behavior of Sands under Seismic Loading Conditions." PhD diss., University of California, Berkeley, 1969.

Spohn, T., M. Grott, S. E. Smrekar, J. Knollenberg, T. L. Hudson, C. Krause, N. Muller, et al. 2018. "The Heat Flow and Physical Properties Package (HP^3) for the InSight Mission." *Space Science Reviews* 214, no. 5 (August): 96. https://doi.org/10.1007/s11214-018-0531-4

TA Instruments. 2006. *AR 2000 Rheometer: Rheometric Series Operator's Manual*. New Castle, DE: TA Instruments.

Villacreses, J. P., B. Caicedo, S. Caro, and F. Yépez. 2020. "A Novel Procedure to Determine Shear Dynamic Modulus and Damping Ratio for Partial Saturated Compacted Fine-Grained Soils." *Soil Dynamics and Earthquake Engineering* 131 (April): 106029. https://doi.org/10.1016/j.soildyn.2019.106029

Vucetic, M. and R. Dobry. 1991. "Effect of Soil Plasticity on Cyclic Response." *Journal of Geotechnical Engineering* 117, no. 1 (January): 89–107. https://doi.org/10.1061/(ASCE)0733-9410(1991)117:1(89)

Weissman, G. F. and R. R. Hart. 1962. "The Damping Capacity of Some Granular Soils." In *Proceedings of the Symposium on Soil Dynamics*, 45–54. West Conshohocken, PA: ASTM International. https://doi.org/10.1520/STP44376S

Wichtmann, T. "Soil Behaviour under Cyclic Loading-Experimental Observations, Constitutive Description and Applications." PhD diss., Karlsruhe Institute for Technology, 2016.